Marine Pollution Bulletin 193 (2023) 115206

Contents lists available at ScienceDirect

Marine Pollution Bulletin

journal homepage: www.elsevier.com/locate/marpolbul

Low environmental impact remediation of microplastics: Visible-light photocatalytic degradation of PET microplastics using bio-inspired C, N-TiO_2/SiO_2 photocatalysts

Maria Camila Ariza-Tarazona [a,b,*], Cristina Siligardi [a,b], Hugo Alejandro Carreón-López [c], José Enrique Valdéz-Cerda [c], Paolo Pozzi [a], Garima Kaushik [e], Juan Francisco Villarreal-Chiu [c,d], Erika Iveth Cedillo-González [a,b,*]

[a] Department of Engineering "Enzo Ferrari", University of Modena and Reggio Emilia, Via P. Vivarelli 10/1, Modena 41125, Italy
[b] National Interuniversity Consortium of Materials Science and Technology (INSTM), Via Giusti, Florence 50121, Italy
[c] Universidad Autónoma de Nuevo León, Facultad de Ciencias Químicas, Av. Universidad S/N Ciudad Universitaria, San Nicolás de los Garza 66455, Nuevo León, Mexico
[d] Centro de Investigación en Biotecnología y Nanotecnología (CIByN), Facultad de Ciencias Químicas, Universidad Autónoma de Nuevo León, Parque de Investigación e Innovación Tecnológica, Km. 10 Autopista al Aeropuerto Internacional Mariano Escobedo, Apodaca 66628, Nuevo León, Mexico
[e] Department of Environmental Science, School of Earth Sciences, Central University of Rajasthan, Ajmer 305817, India

ARTICLE INFO

Keywords:
PET
Photocatalysis
Microplastics
C,N-TiO_2/SiO_2
DSC

ABSTRACT

Microplastics (MPs) are plastic particles with sizes between 1 μm and 5 mm with a ubiquitous presence in aquatic ecosystems. MPs harm marine life and can cause severe health problems for humans. Advanced oxidation processes (AOPs) that involve the in-situ generation of highly oxidant hydroxyl radicals can be an alternative to fight MPs pollution. Of all the AOPs, photocatalysis has been proven a clean technology to overcome microplastic pollution. This work proposes novel C,N-TiO_2/SiO_2 photocatalysts with proper visible-active properties to degrade polyethylene terephthalate (PET) MPs. Photocatalysis was performed in an aqueous medium and at room temperature, evaluating the influence of two pH values (pH 6 and 8). The results demonstrated that the degradation of the PET MPs by C,N-TiO_2/SiO_2 semiconductors is possible, achieving mass losses between 9.35 and 16.22 %.

1. Introduction

Plastics in the ocean are one of the most pressing environmental issues of the current century. Plastic bags, six-pack rings, or ghost nets cause entanglement and asphyxia of the marine biota (Lacerda et al., 2019). The harmful effects of those and other big plastic items in the marine environment are readily visible. However, since 2010, the scientific community has started to keep records of the smaller plastic debris, the so-called microplastics (MPs). MPs are plastics with sizes between 1 μm and 5 mm that were intentionally fabricated in those sizes or that, more often, come from the breakdown of larger plastic items (Wang et al., 2021). Due to their high area-to-volume ratio and surface chemical properties, MPs adsorb persistent organic pollutants (POPs) when they are present in contaminated aquatic environments (Costigan et al., 2022). Marine biota frequently consumes MPs, which promotes physical damage to their tissues by direct contact (Hale et al., 2020) and other general health issues caused when MPs act as POPs vectors in the body (Bhatt and Chauhan, 2023). MPs represent a severe ecological problem as it is well-known that these tiny plastic particles are being transferred through the trophic web. Thus, their presence has recently been confirmed in humans (Ragusa et al., 2021; Schwabl et al., 2019).

Formerly, it was assumed that MPs remain inactive in oceans once released. However, studies revealed that they could be transferred to the atmosphere by sea spray (Allen et al., 2020). MPs are already so ubiquitous that, similar to global biogeochemical cycles, they now spiral around the globe with different atmospheric, oceanic, cryospheric and terrestrial residence times (Brahney et al., 2021).

Due to the previous arguments, MPs are considered an emergent pollutant of global concern, and there is an urgent need for

* Corresponding authors at: Department of Engineering "Enzo Ferrari", University of Modena and Reggio Emilia, Via P. Vivarelli 10/1, Modena 41125, Italy.
E-mail addresses: mariacamila.arizatarazona@unimore.it (M.C. Ariza-Tarazona), ecedillo@unimore.it (E.I. Cedillo-González).

https://doi.org/10.1016/j.marpolbul.2023.115206
Received 31 October 2022; Received in revised form 22 May 2023; Accepted 18 June 2023
Available online 29 June 2023

technological solutions to solve MP pollution. The ocean not only acts as an MPs' sink but has already become a source; a logical approach to fighting MPs pollution is stopping their inputs into the ocean. A feasible and relatively straightforward approach to accomplish this goal is to effectively eliminate the MPs in wastewater effluents before they discharge into water bodies. This approach is based on the fact that wastewater treatment plants (WWTPs) have been identified as a MPs source in aquatic and terrestrial environments (Barceló and Picó, 2019; Sharma et al., 2020). Photocatalysis is a water treatment process that can be adapted as tertiary treatment into WWTPs. By photocatalysis, MPs can be mineralized to CO_2 and H_2O or degraded into molecular species that are expected to be either less toxic (Jiang et al., 2021; Uheida et al., 2021) or short-lived. Furthermore, if performed in visible or solar light and if the photocatalyst is prepared using renewable feedstocks, the overall process respects the sixth, seventh, and ninth principles of Green Chemistry (Jiménez-González and Constable, 2011).

Even though all types of plastics have been found in the marine environment, polyethylene terephthalate (PET) is prevalent in many ecosystems due to its extended use and particular properties. PET is a thermoplastic polyester composed of glycolate and terephthalate subunits connected by ester bonds (Zhang et al., 2021). Together with polypropylene, they represent 26.7 % of worldwide plastic demand (Magalhães et al., 2020), and their applications include bottles for drinking and cleaning products and polyester fibres used in clothing. Indeed, studies indicate that the dominant shape of MPs in WWTPs are microfibres, which have become a significant concern as they are released at every phase of textile production, use and disposal (Arias et al., 2022; Ramasamy et al., 2022). As PET represents a significant proportion of manufacturing textile microfibres (Napper and Thompson, 2016), it has been found in both influents and effluents of WWTPs (Tian et al., 2023; Wu et al., 2022), being considered a dominant polymer in many WWTPs (Xu et al., 2019). PET is predominantly found in the deep sea and sewage works because of its high density compared to other plastics (1.36–1.37 g/cm^3) (Bond et al., 2018) and its high resistance to biodegradation (Mueller, 2006). Hence, this research attempts to degrade this pollutant through a photochemical method and analyze the efficacy of the process through various characterization techniques.

The photocatalytic degradation of PET in an aquatic environment involves two main mechanisms: photo-oxidation and hydrolysis. The hydrolytic degradation of PET strongly depends on the pH and temperature of the surrounding medium (Nguyen-Tri et al., 2014). Even though PET has heteroatoms in the backbone, which are highly susceptible to hydrolysis, aromatic groups make PET highly resistant to degradation under normal conditions (Niaounakis et al., 2019). Because of this, PET hydrolysis is relatively slow, especially at a pH of around 7 (Chamas et al., 2020; Ioakeimidis et al., 2016; Nguyen-Tri and Prud'homme, 2019). It has been reported that in an acidic or alkaline environment, the hydrolysis rate substantially increases (Allen et al., 1994; Edge et al., 1991). In an acidic environment, the protonation of the oxygen atom of the ester group reacts with water to produce hydroxyl and carboxyl end-groups (Allen et al., 1994). In an alkaline environment, the hydroxide anion attacks the carboxyl oxygen atom, producing hydroxyl and carboxyl end-groups (Edge et al., 1991). In this work, the photocatalytic degradation of PET MPs was tested under ambient temperature and two pH values, one slightly acidic (pH 6) and the other slightly alkaline (pH 8), to be closer to natural conditions while also promoting the hydrolytic degradation at non-neutral pH values. Therefore, the goal of this investigation is to present a first step into the implementation of photocatalytic processes for the degradation of microplastics in WWTPs, demonstrating that significant degradation efficiency can be obtained under visible light at ambient temperatures and close-to-neutral pH values without the need for pretreatment of PET MPs (Zhou et al., 2022a).

2. Materials and methods

2.1. C,N-TiO_2/SiO_2 synthesis and characterization

Two C,N-TiO_2/SiO_2 photocatalysts were synthesized using the extrapallial fluid (EPF) of two mussel species. According to Zeng et al. (2015), the EPF of mussels contains proteins that can be used as doping sources (C and N) and pore-forming templates. One C,N-TiO_2/SiO_2 photocatalyst was synthesized using *Mytilus edulis* mussels fluid, referred to as TS-ME, and the other using *Mytilus galloprovincialis* mussels fluid, which will be referred to as TS-MG in this work. The synthesis consisted of two main procedures. The first is a modification from the procedure proposed by Zeng et al. (2015), who intended to obtain a C,N-TiO_2 semiconductor. The methods for extracting the extrapallial fluid and the synthesis process are already described elsewhere (Ariza-Tarazona et al., 2020; Zeng et al., 2015). Briefly, 5 mL of titanium butoxide and 25 mL of extrapallial fluid of *Mytilus edulis* or *Mytilus galloprovincialis* mussels were mixed in a beaker and kept under stirring for 2 h. Then, the mixture was left to mineralize for 4 h without stirring. The second procedure intends to couple the C,N-TiO_2 photocatalyst with SiO_2. In another beaker, 2 mL of tetraethyl orthosilicate and 3.2 mL of isopropyl alcohol were mixed and kept under stirring for 15 min. After that, 0.8 mL of distilled water and 0.10 mL of concentrated nitric acid were added, and the solution was stirred for another 2 h. Further, the contents of both beakers were mixed and stirred for 20 min. The homogeneous mixture was transferred to an autoclave and subjected to a thermal treatment described previously (Ariza-Tarazona et al., 2020; Zeng et al., 2015).

The crystalline structure of the photocatalysts was investigated by X-ray diffraction (XRD), using a Siemens D5000 diffractometer with Cu Kα radiation (accelerating voltage of 40 kV, current of 40 mA, and 2θ-step of 0.023°). The scan was collected between 5 and 80°. The functional groups at the photocatalysts' surface were detected with attenuated total Reflectance-Fourier transform infrared (ATR-FTIR) spectroscopy. The ATR-FTIR spectra were collected using a Vertex 70 ATR-FTIR Bruker spectrometer, averaging 32 scans between 4000 and 400 cm^{-1} with a 4 cm^{-1} spectral resolution. The surface area was estimated by nitrogen adsorption using a Micromeritics TriStar II Plus 3.01 surface area analyzer (analysis bath temperature of 77.3 K, equilibration interval of 5 s, and degasification at 110 °C). The photocatalysts' band gap (E_g) values were calculated from their Diffuse reflectance spectra (DRS). Measures were carried out in the 300–800 nm range on a Jasco V-670 UV–Vis/NIR spectrophotometer equipped with an ILN-725 integration sphere. X-ray photoelectron spectroscopy (XPS) was used to investigate the surface chemistry of the photocatalysts. XPS analyses were carried out using a Thermo Scientific Escalab 250Xi, maintaining a base analysis pressure of ~10–10 mbar; the excitation of the analyzed photoelectrons was performed with a monochromatic X-ray source of Al Kα (1486.68 eV) with an analysis area radius of 650 μm. The analysis conditions for the high-resolution zones were step energy of 20 eV and 45° take-off angle with a step of 0.1 eV. Microstructural characterization was carried out by field emission gun scanning electron microscopy (FEG-SEM) using an FEI Nova Nano SEM 450 instrument.

2.2. PET MPs preparation and characterization

Secondary PET MPs were obtained by grinding a PET food container with a coffee grinder. These particles were then sifted to obtain particles of size ≤500 μm. Their size and morphology were analyzed by optical microscopy (OM) using a Leica EZ4 stereomicroscope. To determine the type of polymer present in the sample, an attenuated total reflectance Fourier transformed infrared spectroscopy (ATR-FTIR) in a Vertex 70 ATR-FTIR Bruker spectrometer was used.

2.3. Photocatalytic degradation experiments

Photocatalytic degradation experiments were performed at room temperature in a closed reaction chamber, where a 50 W LED visible light lamp illuminated the sample from the top. The sample consisted of a Batch-type glass container containing 200 mg of PET MPs and 200 mg of TS-ME or TS-MG in 50 mL of pH 6 or 8 buffer solution. The light irradiance of the lamp was 500 W/m^2 throughout the experiments. The solution was continuously stirred at 350 rpm for 120 h of irradiation. After irradiation, the solution was filtered with a Whatman 40 paper filter, dried at room temperature for 12 h, and then at 50 °C for 2 h in an oven (Fig. 1S, Supplementary Material). The heterogeneous mixture of photocatalyst/PET MPs was weighed, and the weight of the semiconductor was extracted to obtain the remanent weight of the MPs. The photolysis tests followed the same process without the photocatalysts. The degradation was followed by measuring the % of mass loss of the PET MPs according to the following equation:

$$\%\text{Mass loss} = \frac{\text{Initial mass of PET MPs} - \text{Mass of PET MPs at 120 h}}{\text{Initial mass of PET MPs}} \times 100 \quad (1)$$

After measuring the weight of PET and the photocatalytic particles together to calculate the mass loss, a sieving method was used to separate the PET MPs for further characterization. This methodology is often used for characterizing MPs sampled from soil environments (Prata et al., 2019). After that, the PET microplastics were then washed with distilled water and dried at 50 °C for 2 h in an oven before characterization. ATR-FTIR analysis was used to determine the photocatalytic degradation by identifying functional groups formed after 120 h of visible light irradiation. The carbonyl index (CI) was used to assess the degradation of PET MPs. According to the literature, CI was calculated by dividing the absorption of the carbonyl peak (1710 cm^{-1}) by the absorption of the reference band. Reference bands for PET were read at 1504 cm^{-1}, which corresponds to the aromatic ring C═C bond (Piccardo et al., 2020), and at 871 cm^{-1}, which corresponds to the C—H vibrations of the aromatic ring (Janczak et al., 2020).

The crystallinity of PET MPs was studied by differential scanning calorimetry (DSC) to detect alterations in the PET macromolecule because of photocatalytic degradation. The analysis was conducted in a TA Instruments DSC 2010 Differential Scanning Calorimeter in a nitrogen atmosphere. The temperature ranged from 20 to 300 °C with a heating rate of 10 °C/min. The glass transition (T_g), cold crystallization (T_{cc}), and melting temperatures (T_m) were determined. The T_g was obtained at the inflexion point of the heat capacity. The exothermic peak minimum and endothermic peak maximum correspond to T_{cc} and T_m, respectively. The cold crystallization and melting enthalpies were obtained from the area under the curve of their corresponding peaks. The degree of crystallinity (X_c) during the DSC heating stage of the PET MPs was calculated according to the following equation (Mendiburu-Valor et al., 2022):

$$Xc = \frac{\Delta H_m - \Delta H_{cc}}{\Delta H_0} \times 100 \quad (2)$$

where X_c is the degree of crystallinity (%), ΔH_m is the melting enthalpy (J/g), ΔH_{cc} is the cold crystallization enthalpy (J/g), and ΔH_0 is the melting enthalpy for a 100 % crystalline PET (140 J/g) (Loaeza et al., 2021).

The thermal behavior of PET MPs before and after photocatalytic degradation was investigated by thermogravimetric analysis (TGA). TGA measurements were performed in an STA 429 CD Simultaneous thermal analyzer. The measurement temperature range was 50–600 °C, the heating rate was 10 °C/min, and the mass of the samples was around 15 mg. The tests were performed in a helium atmosphere at 50 mL/min.

3. Results and discussion

3.1. C,N-TiO_2/SiO_2 characterization

Fig. 1(a) shows the XRD patterns for the C,N-TiO_2/SiO_2 powders. All the peaks correspond to the anatase TiO_2 and are in accordance with the JCPDS file No. 00–021-1272. As reported earlier, the incorporation of EPF proteins in the synthesis makes the materials amorphous (Ariza-Tarazona et al., 2019, 2020; Zeng et al., 2015). It can be noted that the crystalline structure of TiO_2 is not affected by the incorporation of SiO_2, as the last is in a lower percentage than the detection limit of the instrument, and SiO_2 possibly exists in an amorphous state (Zhang et al., 2019). The FTIR spectrum of the sample is shown in Fig. 1(b). The absorption peaks at 755, and 438 cm^{-1} were attributed to Ti—O and Ti—O—Ti bonds. The broad band at 3500–3200 cm^{-1} was assigned to the stretching vibrations of hydroxyl groups and the bending vibration of the adsorbed H_2O. The absorption peak around 1652 cm^{-1} was referred to the O—H and N—H bonds. The characteristic peak confirms the presence of Si in the samples at 1070 cm^{-1}, attributed to the antisymmetric stretching vibration of the Si—O—Si bond (Zhang et al., 2019). It is also possible that this band overlaps with the band at 1080 cm^{-1}, corresponding to the Ti—N bond. FTIR spectroscopy also detected the symmetric stretching vibration of the Ti—O—Si bond at 956 cm^{-1}. It has been reported that the existence of this bond can improve the photocatalytic activity of the semiconductor since it may lead to the increase of surface defects, resulting in a higher capture of photogenerated carriers and an enhanced activity of the hydroxyl radical (Guo et al., 2014).

The properties of the C,N-TiO_2/SiO_2 photocatalysts are presented in Table 1. The optical properties of the photocatalyst were investigated by UV–Vis diffuse reflectance spectroscopy. The absorbance spectrum is shown in Fig. 2S (Supplementary Material). Using the Kubelka-Munk theory, the E_g values were obtained from the intersection of a straight line from the linear region with the abscissa axis of a plot the $[F(R)h\nu]^{1/2}$ vs. E. The bandgap energy was 2.41 eV and 2.93 for TS-ME and TS-MG, respectively. These values correspond to 514 and 423 nm wavelengths within the visible light threshold. This result suggests that C,N-TiO_2/SiO_2 could have photocatalytic activity under visible light. The reproducibility of the synthesis procedure was investigated using XRD, FTIR and the calculation of the E_g, and is presented in Fig. 3S.

The N_2 adsorption-desorption isotherm is presented in Fig. 1(d). The samples showed a type IV isotherm according to IUPAC, characteristic of mesoporous materials. The hysteresis loop was attributed to H1, indicating that the semiconductor comprises agglomerates of spherical particles. These textural properties of the material explain the high obtained BET surface area of 313 m^2/g for TS-ME and 332 m^2/g for TS-MG. Zeng et al. (2015) synthesized different N-TiO_2 photocatalysts using different concentrations of EPF-derived proteins. Among them, the one with the best physical properties had a 1200 μg/mL concentration. This material had a surface area value three times that of Degussa P25, indicating the positive effect of implementing the EPF from mussels. As they stated, the proteins in this fluid form a 3D network with sites or channels where TiO_2 nuclei can be generated after being mixed with the TiO_2 precursor (titanium tetrabutoxide) and then kept at rest for 4 h. After being subjected to thermal treatment, the proteins were removed, leaving a porous structure of N-TiO_2 with a high surface area. For the C, N-TiO_2 material that was synthesized in our previous work using *Mytilus edulis* mussels (Ariza-Tarazona et al., 2020), the superficial area value is four times than the one of Degussa P25, while for the C,N-TiO_2/SiO_2 synthesized in this work is up to five times the superficial area of Degussa P25. The differences in the increase in surface area between the semiconductors synthesized using *Mytilus edulis* (TS-ME) and *Mytilus galloprovincialis* (TS-MG) mussels and the semiconductor synthesized by Zeng et al. (2015) can be attributed to the different properties of the species of mussels used.

The photocatalyst surface was also analyzed using X-ray photoelectron spectroscopy (XPS). The XPS survey in Fig. 2(a) and (e) confirms the

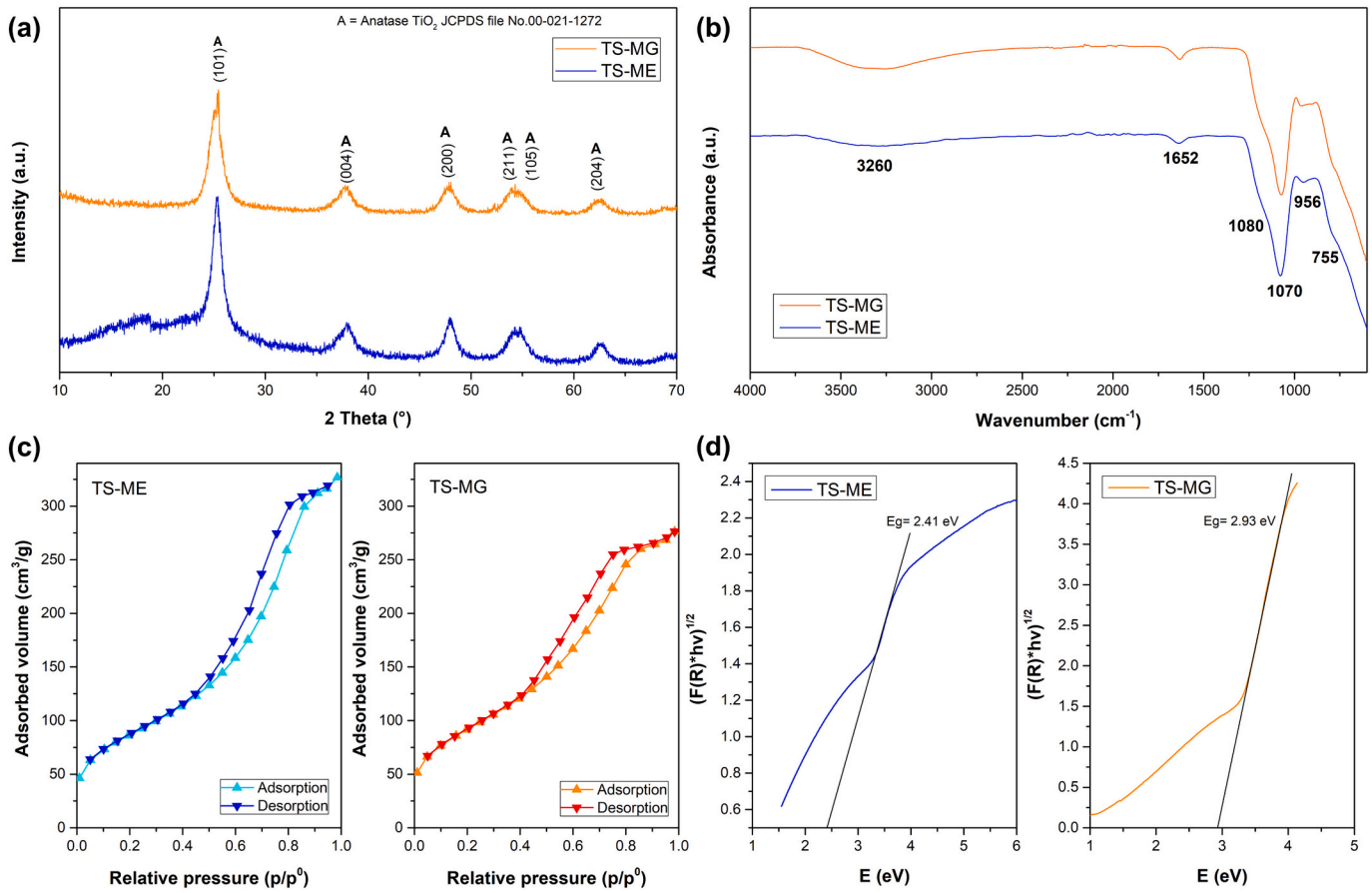

Fig. 1. (a) XRD patterns, (b) ATR-FTIR spectra, (c) nitrogen adsorption isotherms, and (d) Eg calculation for TS-MG and TS-ME samples.

Table 1
Properties of the C,N-TiO_2/SiO_2 photocatalysts using the extrapallial fluid of different species of mussels as a doping source.

Sample	E_g (eV)	Activation wavelength (nm)	S_{BET} (m^2/g)
TS-ME	2.41	514	313
TS-MG	2.93	423	332

presence of O, Ti, Si, N, and C elements. The O 1s spectrum exhibits two peaks for TS-ME (Fig. 2(b) and one peak for TS-MG (Fig. 2(h)). The peak at 532.96 eV may be attributed to Ti-O-Si species (Aman et al., 2016) that had been already identified according to the FTIR spectrum of the sample, while the peaks at around 530 eV are ascribed to the O in the Ti—O—Ti lattice. The spectrum for Ti 2p presents two peaks at around 458 and 464 eV for both samples, corresponding to Ti $2p_{3/2}$ and Ti $2p_{1/2}$, respectively (Zeng et al., 2015). N 1s XPS spectra of TS-ME (Fig. 2b) show a broad peak at 400 eV, suggesting an interstitial nitrogen dopant (Ang et al., 2009), while for TS-MG (Fig. 2(f)), a N 1s peak is detected at 396 eV, suggesting that the nitrogen is found in a substitutional position (Zeng et al., 2015). In the spectrum of C element, for TS-ME (Fig. 2(c)), two peaks were identified at 288.75 and 284.88 eV, which are attributed to sp2 hybridization in CNOs or C of Ti—O—C bonds and the C═O in CNOs, respectively (Zhang et al., 2019), while TS-MG (Fig. 2(g)) presents a broad peak from 288.80 eV to 285.26 eV, suggesting the two peaks mentioned above are overlapped. In the XPS spectrum of Si 2p for both samples (Fig. 2(d) and (h)), one peak was observed at around 103 eV, which may be attributed to Si—O—Si (Zhang et al., 2019).

FEG-SEM micrographs for both photocatalysts are presented in Fig. 3. It can be noted that the photocatalysts are composed of two different morphologies with the same chemical composition (EDX, Figs. 4S and 5S). The first is a 3D network (Fig. 3(a)–(b) and (e)–(f)) of TiO_2, in which the proteins served as templates to generate porosity. The second one is formed by agglomerates of spherical particles that also contribute to increasing the porosity of the C,N-TiO_2/SiO_2 photocatalyst. From Fig. 3, it can be inferred that the 3D network is composed of macropores of diameters between 0.5 and 1.6 μm. In addition, the materials also exhibit agglomerates of 1–3 μm constituted of spherical particles with an average radius of 20–50 nm.

3.2. MPs characterization

The original food container used to obtain the MPs and the characterization of the samples of microplastics obtained after grinding are presented in Fig. 4. The optical microscopy in Fig. 4(b) shows that the sample comprises approximately 200–500 μm sharp microplastic fragments (Fig. 6S). Fig. 4(c) presents the FTIR spectrum of the obtained fragments. According to the literature, the sample presents all main characteristic bands of PET (Piccardo et al., 2020). The band located at 2953 cm^{-1} is assigned to the C—H asymmetric stretching vibrations, while the following bands at 2917 and 2846 cm^{-1} are attributed to the asymmetrical and symmetrical vibrations of CH_2, respectively (Aljoumaa and Abboudi, 2016). The absorption band at 1713 cm^{-1} corresponds to the C═O stretch vibration of the carboxylic ester group, the bands around 1238 to 1092 cm^{-1} are attributed to C—O stretch vibrations, while the bands at 872 and 720 cm^{-1} correspond to the aromatic CH out-of-plane bend (Mendiburu-Valor et al., 2022).

3.3. Photocatalytic degradation tests

The mass loss of PET samples after photocatalysis and photolysis tests with the calculation of the carbonyl index are presented in Table 2.

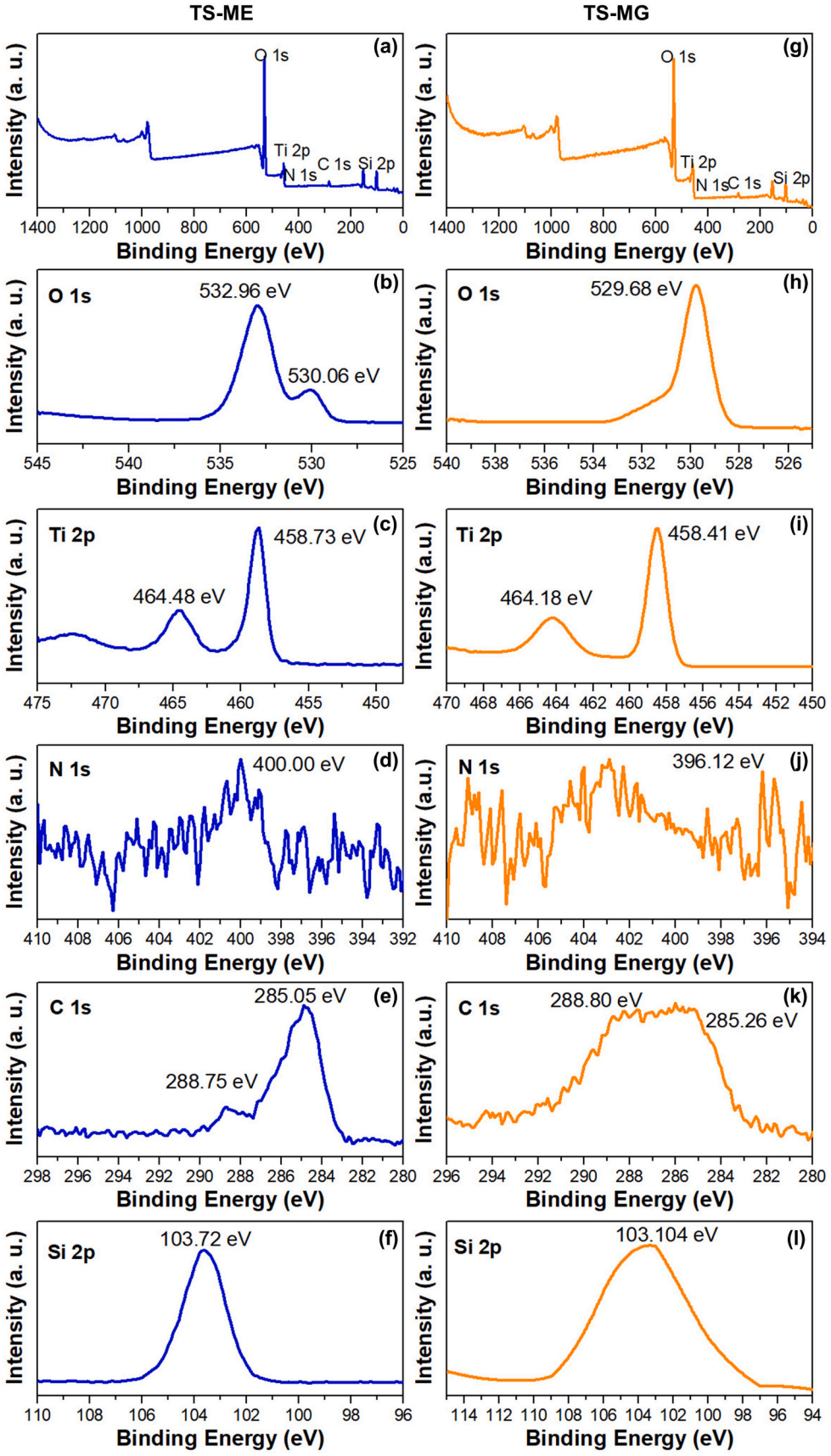

Fig. 2. XPS spectra of TS-ME ((a)–(f)) and TS-MG ((g)–(l)): (a), (g) the survey XPS spectra; (b), (h) O 1s; (d), (j) Ti 2p; (e), (k) C 1s; (f), (l) Si 2p.

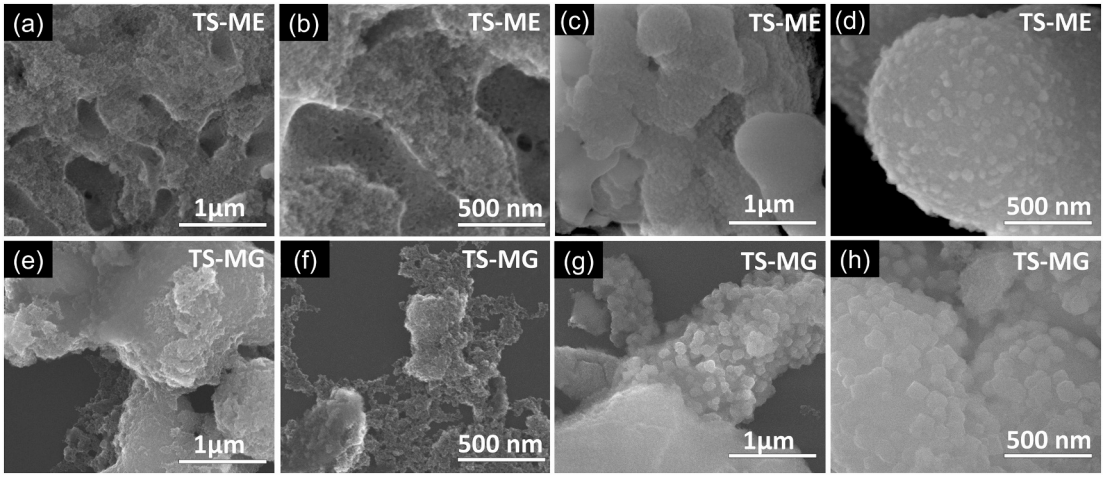

Fig. 3. FEG-SEM micrographs of TS-ME ((a)–(d)) and TS-MG ((e)–(h)) photocatalysts.

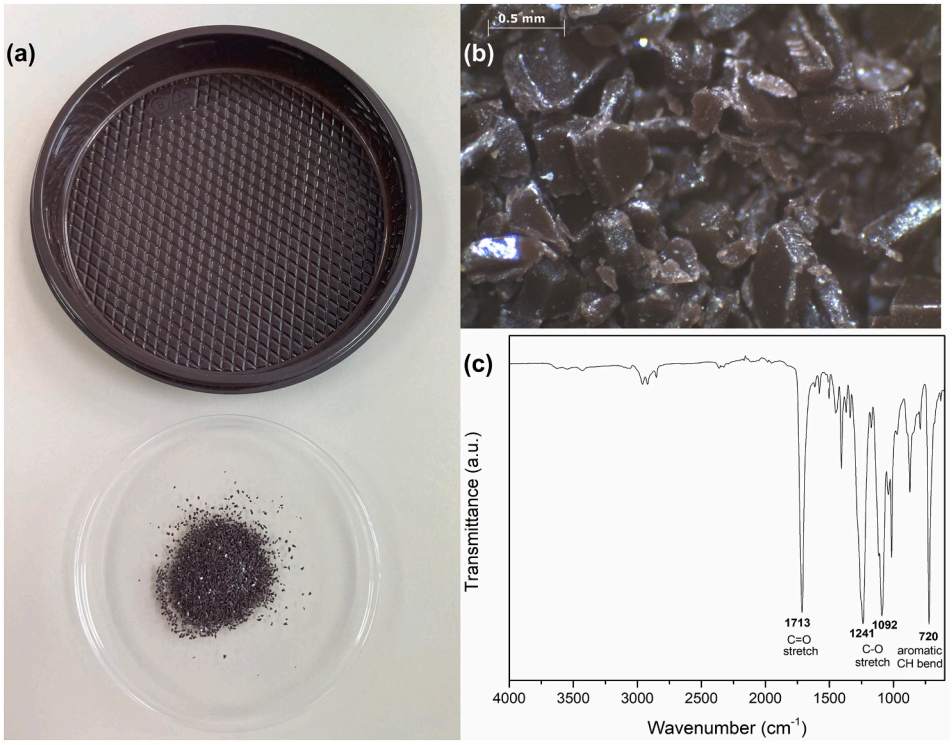

Fig. 4. (a) Original PET container, (b) optical microscopy, and (c) FTIR spectrum of PET MPs.

The mass loss obtained after 120 h of visible light irradiation indicates that the C,N-TiO_2/SiO_2 photocatalysts can degrade PET microplastics at room temperature and pH 6 or 8, achieving mass loss values ranging from 9.35 to 16.22 %. Meanwhile, it was proven that the experiments' conditions do not influence the % of mass loss according to the photolysis experiments. Zhou et al. (2022b) obtained a 10.23 % degradation of PET fibre-based MPs under AM 1.5 irradiation for 48 h. However, a slightly more alkaline pH of 9 was necessary. In another work, Zhou et al. (2022a) reported an approximate 29 % mass loss of PET fibre-based MPs under AM 1.5 irradiation for 48 h. Nonetheless, a hydrothermal pretreatment at 180 °C for 12 h was necessary to induce the initial rough appearance and molecular weight reduction.

The analysis of the bands in the ATR-FTIR spectrum is generally used to study PET degradation as it allows monitoring of chemical changes even at the early stages of degradation (Ferreira et al., 2021). Fig. 5(a) shows the carbonyl band, while Fig. 5(b) shows the spectra from 1500 cm^{-1} to 700 cm^{-1} of PET MPs before and after photocatalytic degradation. The decrease of the band at 1714 cm^{-1} shown in Fig. 5a demonstrated the chain scission of the ester group because of photocatalytic degradation. Fig. 5(b) presents the ATR-FTIR spectra of original and degraded PET samples from 1500 to 700 cm^{-1}. The bands at 1453 and 1407 cm^{-1} are associated with the C—H deformation and the vibration of the phenylene ring, respectively (Aljoumaa and Abboudi, 2016). The bands at 1370 and 1340 cm^{-1} refer to C—H crystalline *gauche* and *trans* conformations, respectively. Meanwhile, the band at 1238 cm^{-1} is designated for asymmetric C—C—O stretching (Mendiburu-Valor et al., 2022). A band at 1220 cm^{-1} developed after irradiation and is associated with the carboxylic acid dimer, as also reported by Horne et al. (Horne et al., 2020). Meanwhile, the bands at 1117 and 1092 cm^{-1} correspond to the *gauche* and *trans* conformation of the ester

Table 2
% of mass loss and CI calculation for PET samples.

Sample	Mass loss (%)	CI(A1714/A1504) (Piccardo et al., 2020)	CI(A1714/A871) (Janczak et al., 2020)
PET original	–	14.12	3.00
PET, TS-ME/pH 6	13.65 ± 0.90	12.77	2.49
PET, TS-MG/pH 6	16.22 ± 7.52	13.86	2.24
PET, TS-ME/pH 8	9.35 ± 0.24	13.98	2.43
PET, TS-MG/pH 8	13.83 ± 0.55	15.05	2.62
PET, Photolysis/pH 6	0.27 ± 0.31	–	–
PET, Photolysis/pH 8	1.39 ± 0.47	–	–

C—O—C stretching, respectively (Aljoumaa and Abboudi, 2016). A decrease in the bands at 1238 and 1092 cm^{-1} correlated with C—O degradation (Piccardo et al., 2020). Furthermore, the band at 1015 cm^{-1}, attributed to the in-plane bending of C—H in the benzene ring, is also directly related to PET crystallinity, according to literature (Bertoldo et al., 2010; Cole et al., 2002). The bands at 970 and 898 cm^{-1} correspond to the C—H bond stretching of the *trans* and *cis* isomers, respectively (Horne et al., 2020). The bands around 872 and 725 cm^{-1} are attributed to the aromatic C—H out-of-plane bending and wagging (Aljoumaa and Abboudi, 2016). However, there is no development of new bands in the stretching vibration of the hydroxyl group or in the region associated with the O—H stretching vibration of ethylene end groups (3615–3115 cm^{-1}), as presented in Fig. 7S. The development of these bands is associated with the formation of carboxylic and alcoholic end groups due to the photochemical and hydrolytic degradation of the polymer (Ioakeimidis et al., 2016; Mendiburu-Valor et al., 2022; Miranda et al., 2021). Also, at later stages of degradation, additional bands start to form in the region from 1705 to 1685 cm^{-1} assigned to the formation of a carboxylic acid dimer, end groups, terephthalic acid monomer, and quinone species (Horne et al., 2020). An explanation for why these bands were not detected in the FTIR spectra could be that the investigated pH conditions can either neutralize these compounds or release them from the MPs surface, therefore not being detected, but further research is needed to confirm this hypothesis.

The carbonyl index (CI) was used to indicate the degree of MPs' degradation. In general, during the photo-oxidation of hydrocarbons, carbonyl groups are generated as the photooxidative degradation progresses, increasing the CI values after degradation. Therefore, higher CI values are expected after a photodegradation process. However, PET polymer already contains carbonyl groups in its original chemical structure, degraded due to the ester chain scission (Ioakeimidis et al., 2016), resulting in lower CI values. Moreover, to make CI analysis more complex, a standard method for determining CI is not currently available, and many different methods are reported in the scientific literature. In this work, CI was determined by calculating the ratio between the absorbance of the carbonyl band at 1714 cm^{-1} and the absorbance of two selected unalterable bands: 1504 cm^{-1} (vibration of the aromatic ring C═C bond) and 871 cm^{-1} (which corresponds to the vibrations of C—H in an aromatic ring). As observed in Table 2, both methods resulted in the same general trend. At pH 6, the decrease in the original PET's CI value after performing photocatalysis suggests that the reaction system is promoting the chain scission of the ester group. However, when pH increases and photocatalysis is performed in an alkaline medium (pH 8), the higher CI values suggest a decreased photocatalytic process efficiency. Such a trend may be related to different degradation paths according to the pH of the reaction medium. For instance, Table 2 shows that the CI values calculated by both methods for sample TS-MG are higher at pH 8 than at pH 6. A hypothesis that can explain this behavior is the formation of photocatalytic degradation products in alkaline conditions containing C═O bonds (carboxylic acids, aldehydes, esters) that remain adsorbed on PET MPs.

In contrast, an acid medium promotes the degradation of such products or release from MPs surface. A similar trend was observed for sample TS-ME using Piccardo's CI calculation method. However, further research is needed to confirm or refute this hypothesis.

DSC analysis was used to investigate the response of PET MPs to heating before and after photocatalytic degradation. In particular, the glass transition temperature (T_g), the cold crystallization temperature (T_{cc}), and the melting temperature were obtained for the heating stage. In contrast, the crystallization temperature (T_c) was obtained for the cooling stage. In addition, PET MPs' degree of crystallinity (X_c) was also determined for both stages as it can give information on a polymer's mechanical properties, stability, and chemical resistance (Kong and Hay, 2002).

The heating stage of DSC analysis for PET MPs is presented in Fig. 6 (a). As can be noted, there are differences in the values of the glass transition temperature (T_g), the cold crystallization temperature (T_{cc}), and the melting temperature (T_m) (values are displayed in Table 3). According to Fig. 6(a), the T_g values of PET MPs after photocatalytic degradation are significantly higher, and their associated peaks become more intense than the T_g values of original PET MPs. This phenomenon is attributed to the relaxation process of the amorphous region of PET MPs

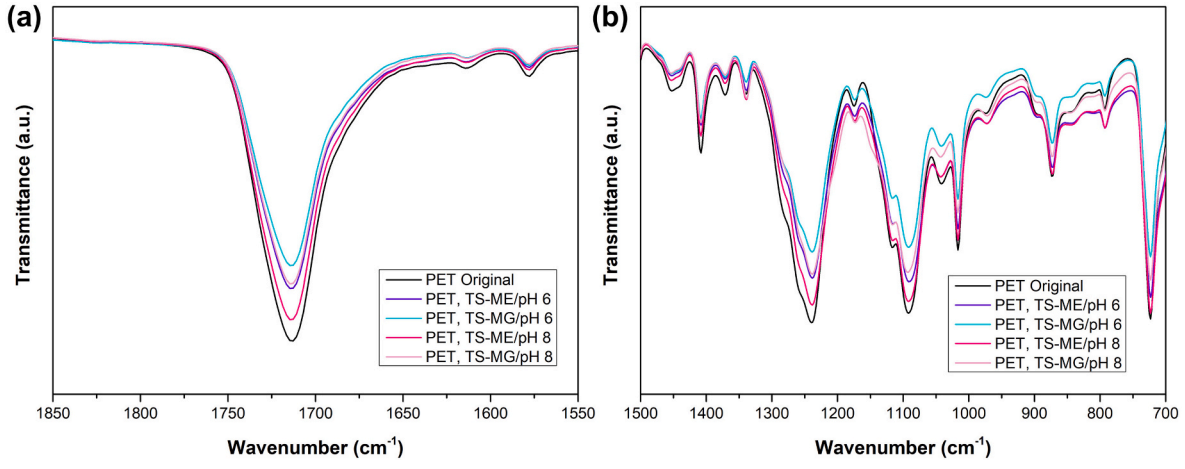

Fig. 5. ATR-FTIR spectra of original PET MPs in the regions between (a) 1850–1550 cm^{-1} (carbonyl region) and (b) 1500–700 cm^{-1}.

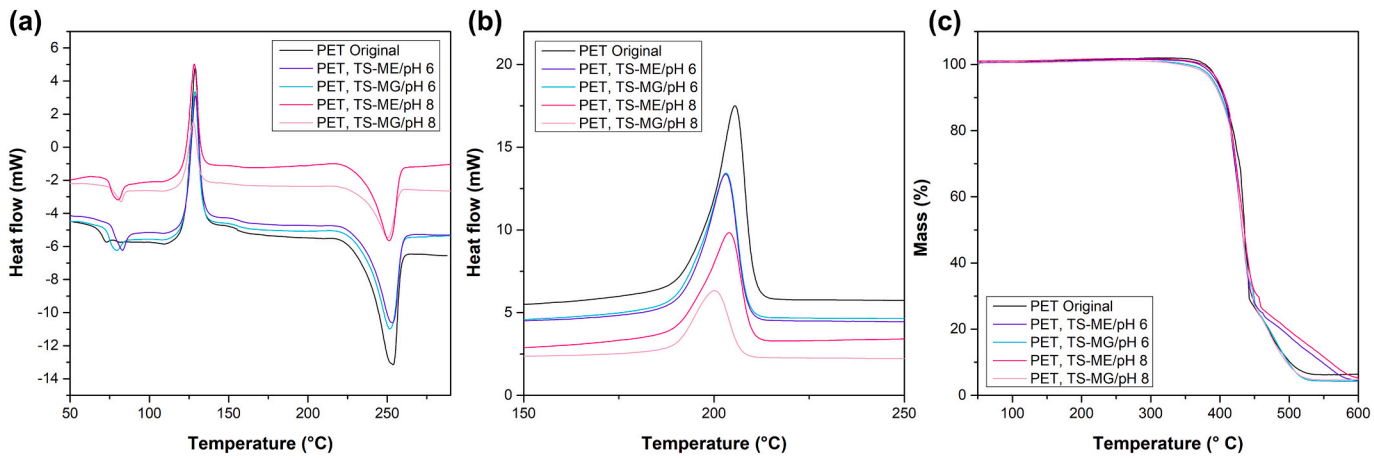

Fig. 6. (a) DSC heating scans, (b) DSC cooling scans, and (c) TGA weight loss curves of different PET MPs samples.

Table 3
Thermal properties of PET MPs before and after photocatalytic degradation.

Sample	Heating				Cooling		T_{onset} (°C)
	T_g (°C)	T_{cc} (°C)	T_m (°C)	X_c (%)	T_c (°C)	X_c (%)	
PET original	73.0	129.0	254.0	9.1	206.0	28.5	418.0
PET, TS-ME/pH 6	83.0	129.1	253.1	5.3	203.1	21.3	407.6
PET, TS-MG/pH 6	79.0	128.8	251.6	5.7	203.2	22.8	403.4
PET, TS-ME/pH 8	79.8	128.3	251.1	4.9	204.0	17.3	406.4
PET, TS-MG/pH 8	82.0	127.8	250.4	2.8	200.1	10.8	405.1

resulting from the mobility of the molecules segments. Meanwhile, the cold crystallization peaks, associated with rearranging the amorphous phase into a crystal phase during DSC heating (Fechine et al., 2002), are slightly lower after the photocatalytic degradation of PET MPs. The second thermal transition observed corresponds to the melting temperature. The obtained T_m values after photocatalytic degradation are slightly lower than the one of the original PET, which demonstrates lower thermo-oxidative stability (Bikiaris and Karayannidis, 1999).

In the cooling scan depicted in Fig. 6(b), the original PET MPs showed a pronounced peak associated with the crystallization process of PET. However, the peak of the degraded MPs was considerably less intense and appeared at lower temperatures than the original MPs, as exhibited in Table 3. The decrease in T_c can be associated with structural changes resulting in structural disorder, which could be attributed to branching and crosslinking reactions (Horne et al., 2020).

The degree of crystallinity calculated from Eq. 2 is also presented in Table 3. The degree of crystallinity, also known as the crystallinity index, is often used as an indicator of the degradation of PET (Hagihara et al., 2014). The degree of crystallinity obtained for the samples subjected to photocatalytic degradation at pH 6 and 8 under visible irradiation shows a marked decrease compared to original PET MPs. This effect has been reported before in literature (Fechine et al., 2002; Miranda et al., 2021; Nguyen-Tri and Prud'homme, 2019; Niaounakis et al., 2019) but is also in disagreement with other works which have reported the opposite effect (Arhant et al., 2019; Farhoodi et al., 2012). To understand this phenomenon, it is important to identify the degradation process that the polymer is going through. PET's most relevant degradation mechanisms include photo-oxidation and thermal and hydrolytic degradation (Fotopoulou and Karapanagioti, 2017).

In this work, the main pathway for the degradation of PET MPs is visible light-induced photo-oxidation. However, as the experiments are performed in an aquatic environment, it is possible that hydrolysis can also take place. During the photo-oxidation of PET, it is expected that a chemi-crystallization process will occur. This process consists of the reorganization of the amorphous phase into a crystalline phase because of the chain scission during degradation, leading to an increase in crystallinity (Arhant et al., 2019; Fechine et al., 2002). Since the rearrangement of the molecules depends on their mobility, the chemi-crystallization process is expected to occur only at temperatures higher than the glass transition temperature (T_g) (Fechine et al., 2002). However, it has been proven that the chemi-crystallization process can occur even at temperatures below the T_g if the environment contains moisture, as the water can act as a plasticizer, promoting molecular mobility (Fechine et al., 2002). Hydrolysis occurs when the water diffuses into the amorphous regions of the polymer, leaving the crystalline regions untouched because of its impermeability to water (Fotopoulou and Karapanagioti, 2017; Sang et al., 2020) and therefore increasing the crystallinity of PET.

Nonetheless, as indicated earlier, a decrease in crystallinity in aquatic environments, as investigated in this work, has been previously reported (Nguyen-Tri and Prud'homme, 2019; Niaounakis et al., 2019). An explanation could be that PET absorbs light causing chain scission within its crystalline regions (Sang et al., 2020). Nevertheless, further research is needed to determine the factors that promote one degradation pathway over the other when hydrolytic degradation and photo-oxidation are combined.

Thermogravimetric analysis was used to study the effect of visible light photocatalytic degradation on the thermal stability of PET MPs at different pH. The thermal curves are presented in Fig. 6(c). and the T_{onset} temperatures for each condition are shown in Table 3. The original PET MPs present good thermostability until around 350 °C when thermal degradation occurs. However, PET MPs that underwent a photocatalytic degradation process showed a decrease in the degradation temperature and T_{onset}. This is attributed to the chain scission resulting from photocatalytic degradation, causing a decline in the molar mass and polymer embrittlement, reducing the PET MPs' thermal stability (Lee et al., 2012; Pires et al., 2015). All the samples exhibited a two-step thermal degradation. The primary step occurs between 300 and 450 °C and corresponds to the ester linkage decomposition due to chain scission, generating vinyl- and carboxy-terminated chain fragments (Achagri

et al., 2020). The secondary step starts at 600 °C and corresponds to C—C bond cleavage, forming volatile compounds (Achagri et al., 2020).

SEM micrographs of the PET MPs were taken to investigate the changes in morphology due to photocatalytic degradation. For this study, PET MPs were obtained from the grinding of a PET food container, leaving cuts on the surface of the samples because of the use of blades in the fragmentation process, which would limit the analysis of the samples using SEM (Fig. 8S). Therefore, we analyzed the samples from the surfaces that were not cut by the blades and remained intact. As can be noted from Fig. 7, the original PET MPs exhibit a uniform flat

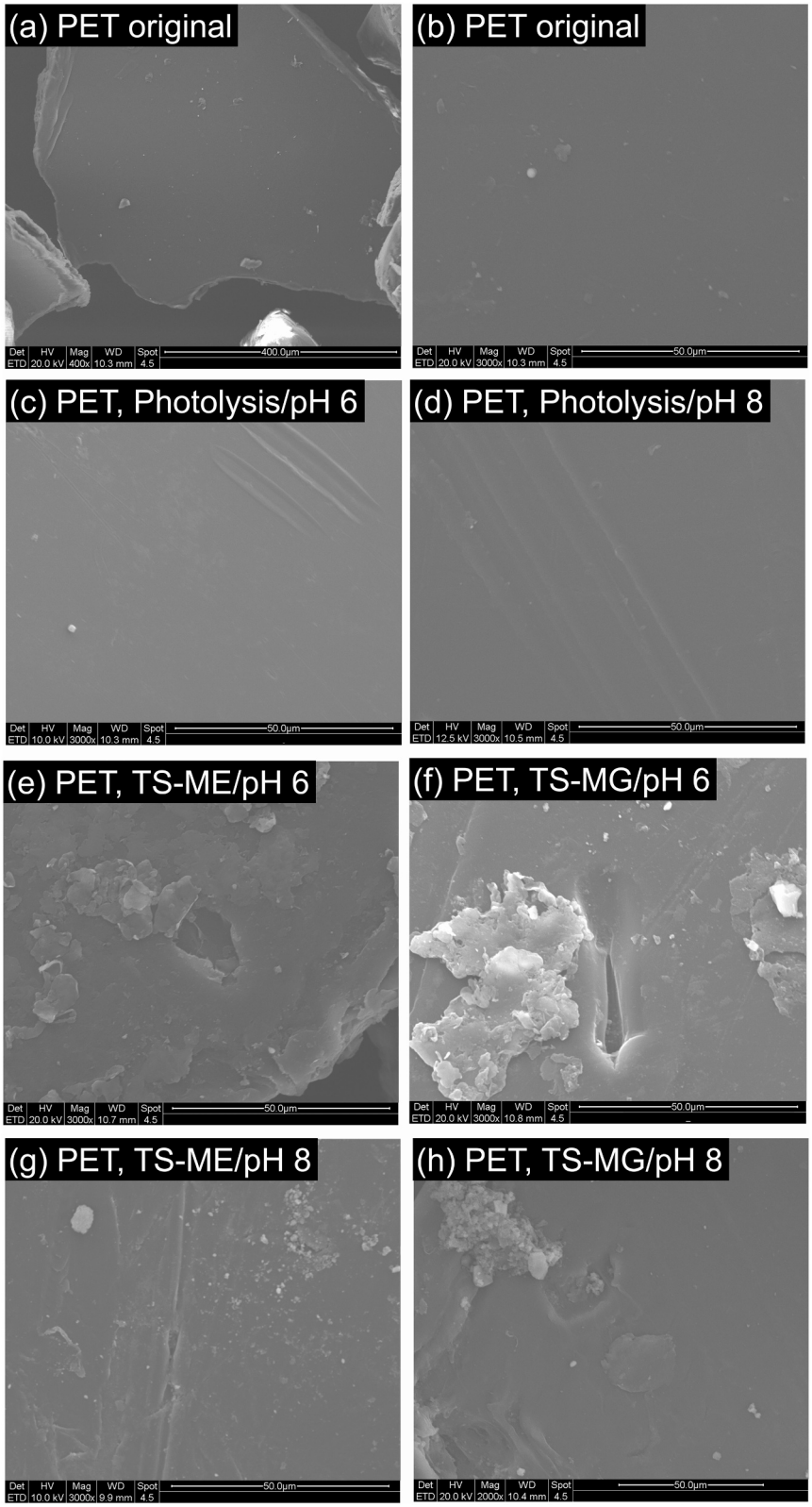

Fig. 7. SEM micrographs of PET MPs (a)–(b) before photocatalytic degradation; (c)–(d) after photolysis; (e)–(h) after 120 h of irradiation with different photocatalysts and pH.

surface, which was not significantly altered after the photolysis. However, after the PET microplastics were exposed to a photocatalytic treatment using TS-ME and TS-MG photocatalysts and pH 6 and 8, holes and cracks were formed on their surface due to degradation (Horne et al., 2020).

4. Conclusions

This work conducted a photocatalytic degradation using novel protein-based C,N-TiO_2/SiO_2 photocatalysts. It was demonstrated that the photocatalysts have suitable bandgap leading to visible light absorption, photoactivation, and high surface area, making them applicable to work in a wide range of the electromagnetic spectrum and degrade PET MPs. Analysis of the conducted experiments' mass loss and carbonyl index revealed the possibility of degrading fragments of PET size $\leq$500 μm in ambient temperature conditions and pH 6 and 8. According to the obtained results, there is no significant difference in the photocatalytic activity of C,N-TiO_2/SiO_2 photocatalysts if they are synthesized using *Mytilus edulis* or *Mytilus galloprovincialis* extrapallial fluid as a source of carbon and nitrogen doping. This is an outstanding achievement as this synthesis can be performed in different parts of the world where these species are found, and the results would be similar.

CRediT authorship contribution statement

Maria Camila Ariza-Tarazona: Methodology, Investigation, Formal analysis, Writing – original draft, Writing – review & editing. Cristina Siligardi: Writing – review & editing, Supervision, Resources. Hugo Alejandro Carreón-López: Investigation. José Enrique Valdéz-Cerda: Supervision. Paolo Pozzi: Resources; Writing – review & editing. Garima Kaushik: Resources, Writing – review & editing. Juan Francisco Villarreal-Chiu: Methodology, Review & editing, Supervision. Erika Iveth Cedillo-González: Conceptualization, Methodology, Writing – original draft, Writing – review & editing, Supervision, Project administration, Funding acquisition.

Declaration of competing interest

The authors declare no competing financial interest.

Data availability

Data will be made available on request.

Acknowledgments

This work was partially supported by CONACYT [Grant APN-2017/5167].

Appendix A. Supplementary data

Supplementary data to this article can be found online at https://doi.org/10.1016/j.marpolbul.2023.115206.

References

Achagri, G., Essamlali, Y., Amadine, O., Majdoub, M., Chakir, A., Zahouily, M., 2020. Surface modification of highly hydrophobic polyester fabric coated with octadecylamine-functionalized graphene nanosheets. RSC Adv. 10, 24941–24950. https://doi.org/10.1039/D0RA02655G.

Aljoumaa, K., Abboudi, M., 2016. Physical ageing of polyethylene terephthalate under natural sunlight: correlation study between crystallinity and mechanical properties. Appl. Phys. A Mater. Sci. Process. 122, 6. https://doi.org/10.1007/s00339-015-9518-0.

Allen, N.S., Edge, M., Mohammadian, M., Jones, K., 1994. Physicochemical aspects of the environmental degradation of poly(ethylene terephthalate). Polym. Degrad. Stab. 43, 229–237. https://doi.org/10.1016/0141-3910(94)90074-4.

Allen, S., Allen, D., Moss, K., Le Roux, G., Phoenix, V.R., Sonke, J.E., 2020. Examination of the ocean as a source for atmospheric microplastics. PLoS One 15, e0232746. https://doi.org/10.1371/journal.pone.0232746.

Aman, N., Das, N.N., Mishra, T., 2016. Effect of N-doping on visible light activity of TiO_2–SiO_2 mixed oxide photocatalysts. J. Environ. Chem. Eng. 4, 191–196. https://doi.org/10.1016/j.jece.2015.10.037.

Ang, T.P., Toh, C.S., Han, Y.-F., 2009. Synthesis, characterization, and activity of visible-light-driven nitrogen-doped TiO_2−SiO_2 mixed oxide photocatalysts. J. Phys. Chem. C 113, 10560–10567. https://doi.org/10.1021/jp9000658.

Arhant, M., Le Gall, M., Le Gac, P.-Y., Davies, P., 2019. Impact of hydrolytic degradation on mechanical properties of PET — towards an understanding of microplastics formation. Polym. Degrad. Stab. 161, 175–182. https://doi.org/10.1016/j.polymdegradstab. 2019.01.021.

Arias, A.H., Alfonso, M.B., Girones, L., Piccolo, M.C., Marcovecchio, J.E., 2022. Synthetic microfibers and Tyre wear particles pollution in aquatic systems: relevance and mitigation strategies. Environ. Pollut. 295, 118607.

Ariza-Tarazona, M.C., Villarreal-Chiu, J.F., Barbieri, V., Siligardi, C., Cedillo-González, E. I., 2019. New strategy for microplastic degradation: green photocatalysis using a protein-based porous N-TiO_2 semiconductor. In: Ceramics International, a Selection of Papers Presented at CIMTEC 2018, vol. 45, pp. 9618–9624. https://doi.org/10.1016/j.ceramint.2018.10.208.

Ariza-Tarazona, M.C., Villarreal-Chiu, J.F., Hernández-López, J.M., Rivera De la Rosa, J., Barbieri, V., Siligardi, C., Cedillo-González, E.I., 2020. Microplastic pollution reduction by a carbon and nitrogen-doped TiO_2: effect of pH and temperature in the photocatalytic degradation process. J. Hazard. Mater. 395, 122632 https://doi.org/10.1016/j.jhazmat.2020.122632.

Barceló, D., Picó, Y., 2019. Microplastics in the global aquatic environment: analysis, effects, remediation and policy solutions. J. Environ. Chem. Eng. 7, 103421 https://doi.org/10.1016/j.jece.2019.103421.

Bertoldo, M., Labardi, M., Rotella, C., Capaccioli, S., 2010. Enhanced crystallization kinetics in poly(ethylene terephthalate) thin films evidenced by infrared spectroscopy. Polymer 51, 3660–3668. https://doi.org/10.1016/j.polymer.2010.05.040.

Bhatt, V., Chauhan, J.S., 2023. Microplastic in freshwater ecosystem: bioaccumulation, trophic transfer, and biomagnification. Environ. Sci. Pollut. Res. 30, 9389–9400. https://doi.org/10.1007/s11356-022-24529-w.

Bikiaris, D.N., Karayannidis, G.P., 1999. Effect of carboxylic end groups on thermooxidative stability of PET and PBT. Polym. Degrad. Stab. 63, 213–218.

Bond, T., Ferrandiz-Mas, V., Felipe-Sotelo, M., van Sebille, E., 2018. The occurrence and degradation of aquatic plastic litter based on polymer physicochemical properties: a review. Crit. Rev. Environ. Sci. Technol. 48, 685–722. https://doi.org/10.1080/10643389.2018.1483155.

Brahney, J., Mahowald, N., Prank, M., Cornwell, G., Klimont, Z., Matsui, H., Prather, K. A., 2021. Constraining the atmospheric limb of the plastic cycle. Proc. Natl. Acad. Sci. U. S. A. 118 https://doi.org/10.1073/pnas.2020719118.

Chamas, A., Moon, H., Zheng, J., Qiu, Y., Tabassum, T., Jang, J.H., Abu-Omar, M., Scott, S.L., Suh, S., 2020. Degradation rates of plastics in the environment. ACS Sustain. Chem. Eng. 8, 3494–3511. https://doi.org/10.1021/acssuschemeng.9b06635.

Cole, K.C., Ajji, A., Pellerin, É., 2002. New insights into the development of ordered structure in poly(ethylene terephthalate). 1. Results from external reflection infrared spectroscopy. Macromolecules 35, 770–784. https://doi.org/10.1021/ma011492i.

Costigan, E., Collins, A., Hatinoglu, M.D., Bhagat, K., MacRae, J., Perreault, F., Apul, O., 2022. Adsorption of organic pollutants by microplastics: overview of a dissonant literature. J. Hazard. Mater. Adv. 6, 100091 https://doi.org/10.1016/j.hazadv.2022.100091.

Edge, M., Hayes, M., Mohammadian, M., Allen, N.S., Jewitt, T.S., Brems, K., Jones, K., 1991. Aspects of poly(ethylene terephthalate) degradation for archival life and environmental degradation. Polym. Degrad. Stab. 32, 131–153. https://doi.org/10.1016/0141-3910(91)90047-U.

Farhoodi, M., Mousavi, S.M., Sotudeh-Gharebagh, R., Emam-Djomeh, Z., Oromiehie, A., Mansour, H., 2012. A study on physical aging of semicrystalline polyethylene terephthalate below the glass transition point. JART 10. https://doi.org/10.22201/icat.16656423.2012.10.5.360.

Fechine, G.J.M., Souto-Maior, R.M., Rabello, M.S., 2002. Structural changes during photodegradation of poly(ethylene terephthalate). J. Mater. Sci. 37, 4979–4984. https://doi.org/10.1023/A:1021067027612.

Ferreira, M.M., da Silva, E.A., Cotting, F., Lins, V.F.C., 2021. UV weathering and performance of a novel corrosion protective coating on steel made from recycled polyethylene terephthalate (PET). Corros. Eng. Sci. Technol. 56, 199–209. https://doi.org/10.1080/1478422X.2020.1836880.

Fotopoulou, K.N., Karapanagioti, H.K., 2017. Degradation of various plastics in the environment. In: Takada, H., Karapanagioti, H.K. (Eds.), Hazardous Chemicals Associated with Plastics in the Marine Environment. The Handbook of Environmental Chemistry. Springer International Publishing, Cham, pp. 71–92. https://doi.org/10.1007/698_2017_11.

Guo, N., Liang, Y., Lan, S., Liu, L., Ji, G., Gan, S., Zou, H., Xu, X., 2014. Uniform TiO_2–SiO_2 hollow nanospheres: synthesis, characterization and enhanced adsorption–photodegradation of azo dyes and phenol. Appl. Surf. Sci. 305, 562–574. https://doi.org/10.1016/j.apsusc.2014.03.136.

Hagihara, H., Oishi, A., Funabashi, M., Kunioka, M., Suda, H., 2014. Free-volume hole size evaluated by positron annihilation lifetime spectroscopy in the amorphous part of poly(ethylene terephthalate) degraded by a weathering test. Polym. Degrad. Stab. 110, 389–394. https://doi.org/10.1016/j.polymdegradstab. 2014.10.008.

Hale, R.C., Seeley, M.E., La Guardia, M.J., Mai, L., Zeng, E.Y., 2020. A global perspective on microplastics. J. Geophys. Res. Oceans 125, e2018JC014719. https://doi.org/10.1029/2018JC014719.

Horne, F.J., Liggat, J.J., MacDonald, W.A., Sankey, S.W., 2020. Photo-oxidation of poly (ethylene terephthalate) films intended for photovoltaic backsheet. J. Appl. Polym. Sci. 137, 48623. https://doi.org/10.1002/app.48623.

Ioakeimidis, C., Fotopoulou, K.N., Karapanagioti, H.K., Geraga, M., Zeri, C., Papathanassiou, E., Galgani, F., Papatheodorou, G., 2016. The degradation potential of PET bottles in the marine environment: an ATR-FTIR based approach. Sci. Rep. 6, 23501. https://doi.org/10.1038/srep23501.

Janczak, K., Dąbrowska, G.B., Raszkowska-Kaczor, A., Kaczor, D., Hrynkiewicz, K., Richert, A., 2020. Biodegradation of the plastics PLA and PET in cultivated soil with the participation of microorganisms and plants. Int. Biodeterior. Biodegradation 155, 105087. https://doi.org/10.1016/j.ibiod.2020.105087.

Jiang, R., Lu, G., Yan, Z., Liu, J., Wu, D., Wang, Y., 2021. Microplastic degradation by hydroxy-rich bismuth oxychloride. J. Hazard. Mater. 405, 124247 https://doi.org/10.1016/j.jhazmat.2020.124247.

Jiménez-González, C., Constable, D.J.C., 2011. Green Chemistry and Engineering: A Practical Design Approach. John Wiley & Sons.

Kong, Y., Hay, J.N., 2002. The measurement of the crystallinity of polymers by DSC. Polymer 43, 3873–3878. https://doi.org/10.1016/S0032-3861(02)00235-5.

Lacerda, A.L.F., Rodrigues, L.S., van Sebille, E., Rodrigues, F.L., Ribeiro, L., Secchi, E.R., Kessler, F., Proietti, M.C., 2019. Plastics in sea surface waters around the Antarctic Peninsula. Sci. Rep. 9, 3977. https://doi.org/10.1038/s41598-019-40311-4.

Lee, C.O., Chae, B., Kim, S.B., Jung, Y.M., Lee, S.W., 2012. Two-dimensional correlation analysis study of the photodegradation of poly(ethylene terephthalate) film. Vib. Spectrosc. 60, 142–145. https://doi.org/10.1016/j.vibspec.2011.10.013.

Loaeza, D., Cailloux, J., Santana Pérez, O., Sánchez-Soto, M., Maspoch, M., 2021. Impact of titanium dioxide in the mechanical recycling of post-consumer polyethylene terephthalate bottle waste: tensile and fracture behavior. Polymers 13, 310. https://doi.org/10.3390/polym13020310.

Magalhães, S., Alves, L., Medronho, B., Romano, A., Rasteiro, M.G., 2020. Microplastics in ecosystems: from current trends to bio-based removal strategies. Molecules 25, 3954. https://doi.org/10.3390/molecules25173954.

Mendiburu-Valor, E., Mondragon, G., González, N., Kortaberria, G., Martin, L., Eceiza, A., Peña-Rodriguez, C., 2022. Valorization of urban and marine PET waste by optimized chemical recycling. Resour. Conserv. Recycl. 184, 106413 https://doi.org/10.1016/j.resconrec.2022.106413.

Miranda, M.N., Sampaio, M.J., Tavares, P.B., Silva, A.M.T., Pereira, M.F.R., 2021. Aging assessment of microplastics (LDPE, PET and uPVC) under urban environment stressors. Sci. Total Environ. 796, 148914 https://doi.org/10.1016/j.scitotenv.2021.148914.

Mueller, R.-J., 2006. Biological degradation of synthetic polyesters—enzymes as potential catalysts for polyester recycling. From biochemistry. Biochem. Eng. Syst. Biol. 41, 2124–2128. https://doi.org/10.1016/j.procbio.2006.05.018.

Napper, I.E., Thompson, R.C., 2016. Release of synthetic microplastic plastic fibres from domestic washing machines: effects of fabric type and washing conditions. Mar. Pollut. Bull. 112, 39–45. https://doi.org/10.1016/j.marpolbul.2016.09.025.

Nguyen-Tri, P., Prud'homme, R.E., 2019. Nanoscale analysis of the photodegradation of polyester fibers by AFM-IR. J. Photochem. Photobiol. A Chem. 371, 196–204. https://doi.org/10.1016/j.jphotochem.2018.11.017.

Nguyen-Tri, P., El Aidani, R., Leborgne, É., Pham, T., Vu-Khanh, T., 2014. Chemical ageingaging of a polyester nonwoven membrane used in aerosol and drainage filter. Polym. Degrad. Stab. 101, 71–80. https://doi.org/10.1016/j.polymdegradstab.2014.01.001.

Niaounakis, M., Kontou, E., Pispas, S., Kafetzi, M., Giaouzi, D., 2019. Aging of packaging films in the marine environment. Polym. Eng. Sci. 59, E432–E441. https://doi.org/10.1002/pen.25079.

Piccardo, M., Provenza, F., Grazioli, E., Cavallo, A., Terlizzi, A., Renzi, M., 2020. PET microplastics toxicity on marine key species is influenced by pH, particle size and food variations. Sci. Total Environ. 715, 136947 https://doi.org/10.1016/j.scitotenv.2020.136947.

Pires, H.M., Mendes, L.C., Cestari, S.P., Pita, V.J.R.R., 2015. Effect of weathering and accelerated Photoaging on PET/PC (80/20 wt/wt%) melt extruded blend. Mater. Res. 18, 763–768. https://doi.org/10.1590/1516-1439.010115.

Prata, J.C., da Costa, J.P., Duarte, A.C., Rocha-Santos, T., 2019. Methods for sampling and detection of microplastics in water and sediment: a critical review. TrAC Trends Anal. Chem. 110, 150–159. https://doi.org/10.1016/j.trac.2018.10.029.

Ragusa, A., Svelato, A., Santacroce, C., Catalano, P., Notarstefano, V., Carnevali, O., Papa, F., Rongioletti, M.C.A., Baiocco, F., Draghi, S., D'Amore, E., Rinaldo, D., Matta, M., Giorgini, E., 2021. Plasticenta: first evidence of microplastics in human placenta. Environ. Int. 146, 106274 https://doi.org/10.1016/j.envint.2020.106274.

Ramasamy, R., Aragaw, T.A., Balasaraswathi Subramanian, R., 2022. Wastewater treatment plant effluent and microfiber pollution: focus on industry-specific wastewater. Environ. Sci. Pollut. Res. 29, 51211–51233.

Sang, T., Wallis, C.J., Hill, G., Britovsek, G.J.P., 2020. Polyethylene terephthalate degradation under natural and accelerated weathering conditions. Eur. Polym. J. 136, 109873 https://doi.org/10.1016/j.eurpolymj.2020.109873.

Schwabl, P., Köppel, S., Königshofer, P., Bucsics, T., Trauner, M., Reiberger, T., Liebmann, B., 2019. Detection of various microplastics in human stool. Ann. Intern. Med. 171, 453–457. https://doi.org/10.7326/M19-0618.

Sharma, S., Basu, S., Shetti, N.P., Nadagouda, M.N., Aminabhavi, T.M., 2020. Microplastics in the environment: occurrence, perils, and eradication. Chem. Eng. J. 127317 https://doi.org/10.1016/j.cej.2020.127317.

Tian, L., Skoczynska, E., van Putten, R.-J., Leslie, H.A., Gruter, G.-J.M., 2023. Quantification of polyethylene terephthalate micro- and nanoplastics in domestic wastewater using a simple three-step method. Sci. Total Environ. 857, 159209 https://doi.org/10.1016/j.scitotenv.2022.159209.

Uheida, A., Mejía, H.G., Abdel-Rehim, M., Hamd, W., Dutta, J., 2021. Visible light photocatalytic degradation of polypropylene microplastics in a continuous water flow system. J. Hazard. Mater. 406, 124299 https://doi.org/10.1016/j.jhazmat.2020.124299.

Wang, C., Zhao, J., Xing, B., 2021. Environmental source, fate, and toxicity of microplastics. J. Hazard. Mater. 407, 124357 https://doi.org/10.1016/j.jhazmat.2020.124357.

Wu, X., Zhao, X., Chen, R., Liu, P., Liang, W., Wang, J., Teng, M., Wang, X., Gao, S., 2022. Wastewater treatment plants act as essential sources of microplastic formation in aquatic environments: a critical review. Water Res. 221, 118825 https://doi.org/10.1016/j.watres.2022.118825.

Xu, X., Jian, Y., Xue, Y., Hou, Q., Wang, L., 2019. Microplastics in the wastewater treatment plants (WWTPs): occurrence and removal. Chemosphere 235, 1089–1096. https://doi.org/10.1016/j.chemosphere.2019.06.197.

Zeng, H., Xie, J., Xie, H., Su, B.-L., Wang, M., Ping, H., Wang, W., Wang, H., Fu, Z., 2015. Bioprocess-inspired synthesis of hierarchically porous nitrogen-doped TiO_2 with high visible-light photocatalytic activity. J. Mater. Chem. A 3, 19588–19596. https://doi.org/10.1039/C5TA04649A.

Zhang, K., Hamidian, A.H., Tubić, A., Zhang, Y., Fang, J.K.H., Wu, C., Lam, P.K.S., 2021. Understanding plastic degradation and microplastic formation in the environment: a review. Environ. Pollut. 274, 116554 https://doi.org/10.1016/j.envpol.2021.116554.

Zhang, W., Zhang, Y., Yang, K., Yang, Y., Jia, J., Guo, L., 2019. Photocatalytic performance of SiO_2/CNOs/TiO_2 to accelerate the degradation of rhodamine B under visible light. Nanomaterials 9, 1671. https://doi.org/10.3390/nano9121671.

Zhou, D., Luo, H., Zhang, F., Wu, J., Yang, J., Wang, H., 2022a. Efficient photocatalytic degradation of the persistent PET Fiber-based microplastics over Pt nanoparticles decorated N-doped TiO_2 Nanoflowers. Adv. Fiber Mater. 1–14 https://doi.org/10.1007/s42765-022-00149-4.

Zhou, D., Wang, L., Zhang, F., Wu, J., Wang, H., Yang, J., 2022b. Feasible degradation of polyethylene terephthalate fiber-based microplastics in alkaline media with Bi_2O_3@N-TiO_2 Z-scheme photocatalytic system. Adv. Sustain. Syst. 6, 2100516. https://doi.org/10.1002/adsu.202100516.